Unexpected Direct Synthesis of Tunable Redox-Active Benzil-Linked Polymers via the Benzoin Reaction

Christina Cong,‡ Jaehwan Kim,‡ Cara N. Gannett, Héctor D. Abruña, Phillip J. Milner*

Department of Chemistry and Chemical Biology, Cornell University, Ithaca, NY, 14850, United States

ABSTRACT: Strategies for the sustainable synthesis of redox-active organic polymers could lead to next-generation organic electrode materials for electrochemical energy storage, electrocatalysis, and electro-swing chemical separations. Among redox-active moieties, benzils or aromatic 1,2-diones are particularly attractive due to their high theoretical gravimetric capacities and fast charge/discharge rates. Herein, we demonstrate that the cyanide-catalyzed polymerization of simple dialdehyde monomers unexpectedly leads to insoluble redox-active benzil-linked polymers instead of the expected benzoin polymers, as supported by solid-state nuclear magnetic resonance spectroscopy and electrochemical characterization. Mechanistic studies suggest that cyanide-mediated benzoin oxidation occurs by hydride transfer to the solvent, and that the insolubility of the benzil-linked polymers protects them from subsequent cyanolysis. The thiophene-based polymer **poly(BTDA)** is an intriguing organic electrode material that demonstrates two reversible one-electron reductions with monovalent cations such as Li^+ and Na^+ but one two-electron reduction with divalent Mg^{2+}. As such, the tandem benzoin-oxidation polymerization reported herein represents a sustainable method for the synthesis of highly tunable and redox-active organic materials.

INTRODUCTION

Greenhouse gas emissions are rising rapidly, and as a result the world must rapidly transition towards more renewable and sustainable processes, particularly in the chemical manufacturing and energy production/storage sectors.[1,2] Key to these efforts are redox-active materials, which are required for applications ranging from heterogeneous electrocatalysis to electrochemical energy storage to electro-swing carbon capture.[3–9] As such, the development of flexible, lightweight, high-capacity, and tunable redox-active materials is required to meet increasing global sustainability demands.

Crystalline inorganic solids, such as $LiCoO_2$ electrodes for lithium-ion batteries (LIBs) and Cu-based electrodes for electrocatalytic CO_2 conversion, currently dominate industrial applications of redox-active materials.[10–12] However, these materials suffer from several fundamental shortcomings, including low power densities, the use of scarce elements, lack of tunability, and large carbon footprints due to unsustainable manufacturing and mining processes.[12–14] For example, the crystalline inorganic cathodes employed in LIBs suffer from slow intercalation of charge-balancing cations, restricting their capacities at fast charge/discharge rates. Furthermore, the high synthesis temperatures and energy-intensive extraction and refinement procedures involved in the production of inorganic solids lead to significant carbon emissions.[12–15]

Organic electrode materials containing electroactive moieties offer a number of potential advantages over inorganic electrodes, including structural and compositional tunability, improved sustainability, increased flexibility, and faster charge/discharge rate capabilities.[8,9,16–20] These features make organic electrode materials particularly promising for applications requiring high power densities or structural versatility, such as the inclusion of Na^+ or Mg^{2+} ions.[16] However, organic materials have struggled to supplant traditional inorganic electrodes in the context of electrocatalysis[4,5,7–9] and energy storage[15,16] due to several limitations. Beyond challenges associated with solubility and poor electrical conductivity, many redox-active organic polymers are also prepared using expensive precious metal catalysts (*e.g.* Pd), limiting their scalability.[14,17,19,20] Recently, green methods for synthesizing redox-active organic polymers have emerged but remain comparatively limited in scope.[21–25] In addition, the field has coalesced around a small number of redox-active moieties, such as aminoxyl radicals, diimides,

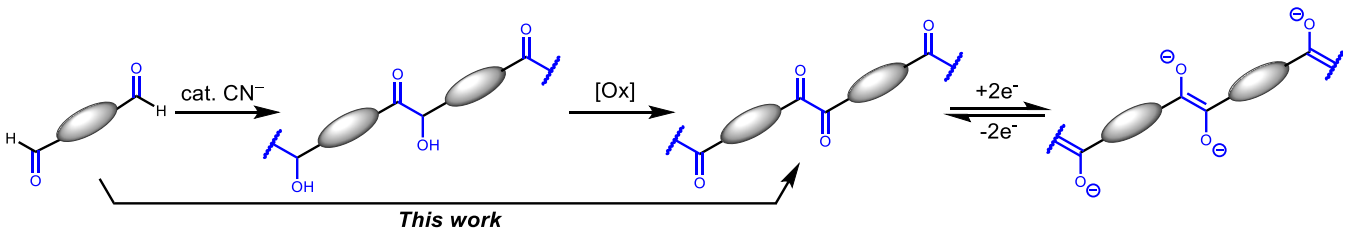

Figure 1. Direct synthesis of redox-active benzil polymers via the benzoin reaction followed by oxidation.

and 1,4-quinones, unnecessarily limiting the design space for organic electrode materials.[16,18,19] Thus, expanding the lexicon of green methods available for the synthesis of polymers functionalized with underdeveloped redox-active moieties would lead to next-generation organic materials for electrocatalysis and energy storage.[20]

Despite their promising features such as high theoretical gravimetric capacities and fast charge/discharge rates with alternative ions such as Mg^{2+} (Figure 1), aromatic 1,2-diones or benzils remain understudied as organic electrode materials.[26–34] This is likely due to the limited methods available for the incorporation of 1,2-diones into polymeric materials, as most methods rely on installing the 1,2-dione into a complex monomer first followed by polymerization. We hypothesize that a straightforward and general route to access polymers linked by aromatic 1,2-diones would be via the benzoin reaction of simple aldehyde monomers[35–37] followed by oxidation of the resulting benzoin moieties (Figure 1).[27,38,39] Although underutilized for the synthesis of polymeric materials,[38,40–42] the benzoin reaction is an attractive method for polymer synthesis due to its atom economy and reversibility, potentially allowing for access to crystalline materials such as covalent organic frameworks (COFs). The requisite metal cyanide (CN^-) salt catalysts, while toxic, are inexpensive and widely used in industry for pharmaceutical synthesis, gold mining, and electroplating.

Herein, we describe the fortuitous discovery that the synthesis of polymers using the cyanide-mediated benzoin reaction under air-free conditions leads directly to a class of insoluble redox-active 1,2-dione-linked polymers without the need for external oxidants, as confirmed by spectroscopic and electrochemical studies. Molecular mechanistic studies suggest that the CN^--mediated oxidation of benzoins to benzils likely occurs via hydride transfer to the protic solvent—a side reaction that has been uninvestigated or overlooked in molecular benzoin reactions. Furthermore, our studies demonstrate that precipitation of the polymer from solution during synthesis is critical to minimize cyanolysis of the formed benzil linkages. Characterization of these redox-active polymers confirms that their redox-activity can be tuned by changing the flanking aryl groups or the charge-balancing cation, and that they retain high charge storage capacities (≥87 mAh/g) at fast discharge rates (1.0 A/g) in lithium metal half cells. Overall, our work represents a sustainable and generalizable method for the synthesis of redox-active organic materials.

RESULTS AND DISCUSSION

Synthesis and characterization of poly(BPDA). We began our investigation into benzoin polymerizations using 4,4′-biphenyldialdehyde (**BPDA**) as a monomer and KCN as a catalyst to prepare a polymer designated as **CORN-BP-1** (CORN = Cornell University, BP = benzoin or benzil polymer) (Figure 2) and referred to here-in as **poly(BPDA)**. Small-scale polymerization reactions were carried out in screw-cap reaction tubes under dry N_2 to minimize competing oxidation of the aldehydes to carboxylic acids.[36] After filtration, the resulting insoluble polymeric materials were soaked in tetrahydrofuran (THF) to remove soluble impurities and dried under vacuum prior to analysis by Attenuated

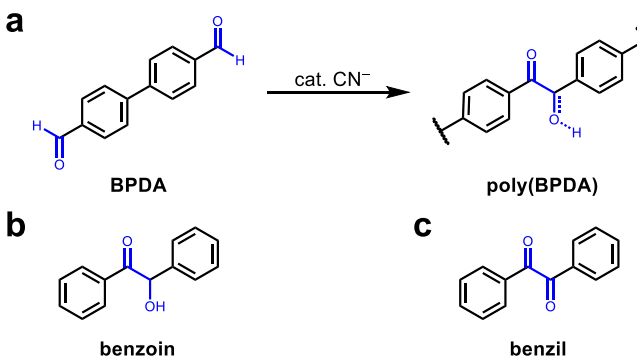

Figure 2. a) Conversion of **BPDA** to benzoin- or benzil-linked polymer **poly(BPDA)** under optimized reaction conditions. Model compounds b) benzoin and c) benzil.

Total Reflectance (ATR) infrared (IR) spectroscopy. In all cases, significant conversion of **BPDA** was confirmed by the disappearance of aldehyde C–H stretches in the ATR-IR spectra of the polymeric samples (see SI section 3 for details).

An extensive evaluation of solvents confirmed that protic solvents, including ethanol (EtOH) and ethylene glycol (EG), produced the highest yields of **poly(BPDA)** (SI Table S1). Among the solvents tested, EG was chosen because it is a green solvent with a high boiling point.[43] Further optimization of the KCN loading, reaction time, and reaction temperature revealed that carrying out the polymerization at 120 °C with 0.50 equivalents of KCN for 96 h was ideal for maximizing the yield of insoluble **poly(BPDA)** (49%) while minimizing the KCN loading (SI Table S2). As such, a bulk sample of **poly(BPDA)** was prepared under these conditions for further structural characterization (Figure 2a; see SI sections 4 and 13 for details).

Characterization of **poly(BPDA)** by scanning electron microscopy (SEM, SI Figures S23–S24), transmission electron microscopy (TEM, SI Figure S31a), scanning tunneling electron microscopy (STEM, SI Figure S31b) and powder X-ray diffraction (PXRD, SI Figure S39) confirmed that it is a microcrystalline polymer. In particular, the observed reflections by PXRD (λ = 1.5406 Å) correspond to d spacings of 4.5 Å (2θ = 19.7 °), 4.2 Å (2θ = 21.1 °) and 3.3 Å (2θ = 27.2 °), suggesting that the limited crystalline order in **poly(BPDA)** likely arises from π–π stacking interactions.[44] Furthermore, TEM confirmed the presence of long (~100 nm) strands, consistent with the expected 1-dimensional polymeric structure of this material (SI Figure S31a). Notably, energy-dispersive X-ray spectroscopy (EDS) and X-ray photon spectroscopy (XPS) established the absence of residual potassium (and thus KCN) in the sample (SI Figures

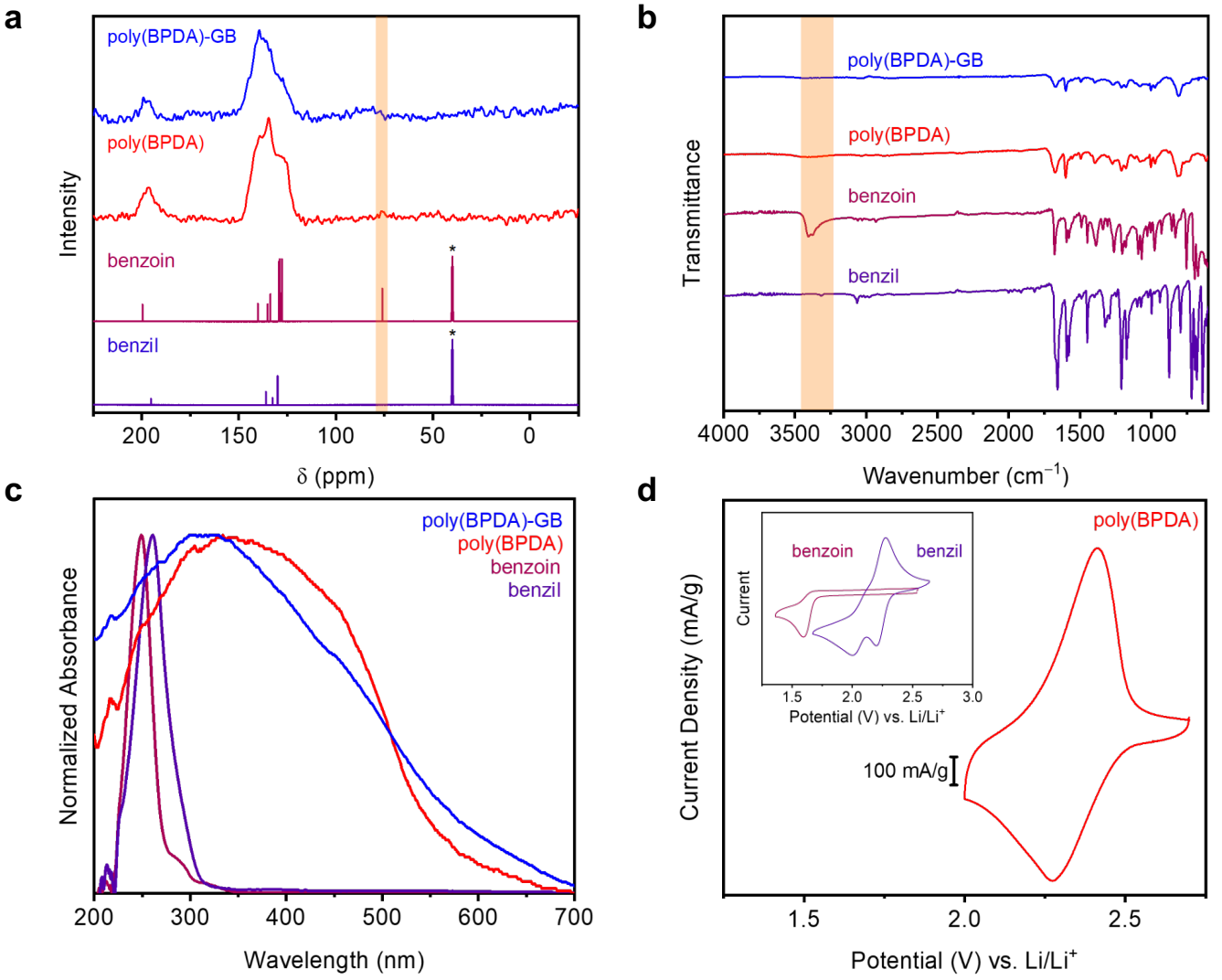

Figure 3. Solid-state spectroscopic characterization of **poly(BPDA)** and **poly(BPDA)-GB** prepared at 120 °C with 0.50 equivalents of KCN for 96 h compared to the model compounds benzoin and benzil. a) CP MAS ^{13}C SSNMR (125 MHz) spectra of the polymers and solution-state ^{13}C NMR (125 MHz, DMSO-d_6) of the model compounds. The peak corresponding to DMSO-d_6 is indicated (*). SSNMR spectra were collected at a spinning speed of 20 kHz with a ^{1}H–^{13}C contact time of 1 and 4 ms for **poly(BPDA)-GB** and **poly(BPDA)**, respectively. The H–^{13}C–OH resonance of benzoin is highlighted. b) ATR IR spectra of the polymers and model compounds. The O–H stretch of benzoin is highlighted. c) Solid-state UV-Vis absorption spectra of the polymers and solution-state UV-Vis absorption spectra of the model compounds. d) Solid-state CV of **poly(BPDA)** carried out at 1 mV/s in 1 M lithium bis(trifluoromethanesulfonyl)imide (LiTFSI) in dimethyl sulfoxide (DMSO). Inset: solution-state CVs of the model compounds at 1 mM concentration carried out at 50 mV/s in 0.1 M $LiClO_4$ in DMSO.

S25–S26 and S30 and Tables S3 and S5). However, combustion analysis and XPS detected small amounts of incorporated N (≈1%), presumably due to residual nitrile groups resulting from CN^- attack during the benzoin reaction (SI Tables S4–S5 and Figures S26 and S29). Together, these data confirm the conversion of **BPDA** into a polymeric material under the optimized reaction conditions.

Unexpectedly, further characterization of **poly(BPDA)** by cross-polarized magic angle spinning (CP MAS) ^{13}C solid-state nuclear magnetic resonance (SSNMR), ATR-IR, Raman, and solid-state UV-Vis spectroscopies revealed that the initially assigned structure of a benzoin-linked polymer was likely incorrect (Figures 3a–c). Although resonances corresponding to the ketone carbonyl (δ 198 ppm) and aromatic carbons (δ 118–152 ppm) were observed in the CP MAS ^{13}C SSNMR spectrum of **poly(BPDA)**, the H–^{13}C–OH resonance characteristic of the benzoin moiety at approximately δ 76 ppm was consistently not detected (Figure 3a), even at different ^{1}H–^{13}C contact times (SI Figure S35). This is unexpected, as a secondary alcohol carbon bearing a ^{1}H should yield a stronger ^{13}C signal than a quaternary carbonyl carbon in cross-polarization experiments, especially with short ^{1}H–^{13}C contact times.[45] It should be noted that neither esters nor carboxylic acids were detected by CP MAS ^{13}C SSNMR (δ 160–180 ppm) in **poly(BPDA)** as well. Likewise, the ATR-IR spectrum of **poly(BPDA)** lacks peaks near 3300 cm^{-1} corresponding to the alcohol O–H stretch of benzoin (Figure 3b). Last, the solid-state UV-Vis absorption spectrum of **poly(BPDA)** dispersed in $BaSO_4$ displayed a broad absorption peak centered around 350 nm and extending into the

visible region, which is inconsistent with the poor absorbance of benzoin in the visible region (Figure 3c).[41] Indeed, while benzoin is a white solid, **poly(BPDA)** is bright yellow (SI Figure S32), reflecting a greater degree of π-conjugation than would be expected for a non-conjugated polymer.

Based on the characterization data outlined above, we hypothesized that **poly(BPDA)** is actually primarily a benzil-linked polymer instead of the expected benzoin-linked material. Indeed, the CP MAS ^{13}C SSNMR spectrum of **poly(BPDA)** matches well with the corresponding spectra for an authentic sample of benzil (Figure 3a). Consistently, the ^{13}C chemical shift for the carbonyl group in **poly(BPDA)** (δ 196.1 ppm) is closer to that of benzil (δ 194.5 ppm) than to that of benzoin (199.0 ppm) (SI Table S14). As further support, benzil is a light-yellow solid with an absorbance maximum that is bathochromically shifted (λ_{max} = 261 nm) compared to that of benzoin (λ_{max} = 249 nm). Furthermore, benzil displays weak absorbance around 400 nm while benzoin shows no absorbance in the visible region (SI Figures S123–S124). This difference is amplified in the UV-Vis absorption features and the color of **poly(BPDA)** (Figure 3c), as would be expected due to increased cross-conjugation in the polymer. Critically, solid-state cyclic voltammetry (CV) measurements also revealed that **poly(BPDA)** undergoes a reversible reduction at $E_{1/2}$ = 2.274 V vs Li/Li$^+$ (Figure 3d). This finding is consistent with the solution-state redox behavior of benzil, which undergoes a reversible two-electron reduction in certain organic solvents such as *N,N*-dimethylformamide (DMF),[29,46,47] and inconsistent with that of benzoin, which undergoes an irreversible one-electron reduction at more negative potentials (Figure 3d and SI Figures

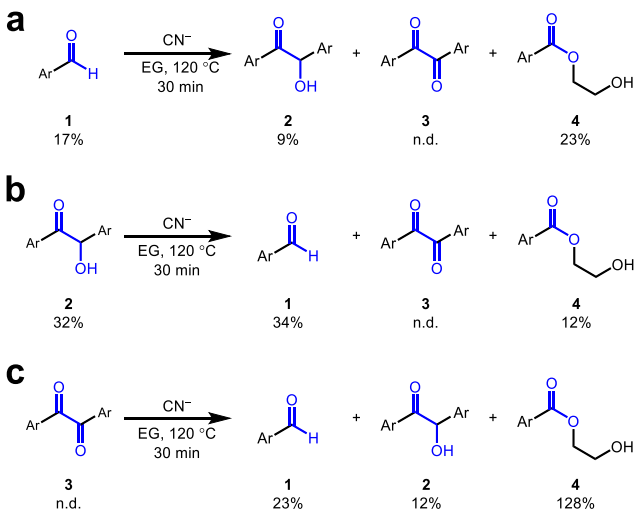

Figure 4. ^{19}F NMR molecular model studies of the CN^--mediated polymerization of **BPDA**. Ar = 3-fluorophenyl.

S129 and S130a). In more polar solvents such as dimethyl sulfoxide (DMSO), benzil undergoes two one-electron reductions separated by a small difference in formal potentials (Figure 3d, SI Figure S130b). Furthermore, the reduction peak positions of benzil (2.157 V vs. Li/Li$^+$) and **poly(BPDA)** (2.274 V vs. Li/Li$^+$) in DMSO are comparable, suggesting that similar redox processes are taking place in both materials (SI Table S10). Although we cannot rule out the presence of trace benzoin linkages in **poly(BPDA)** that cannot be detected spectroscopically, our findings suggest

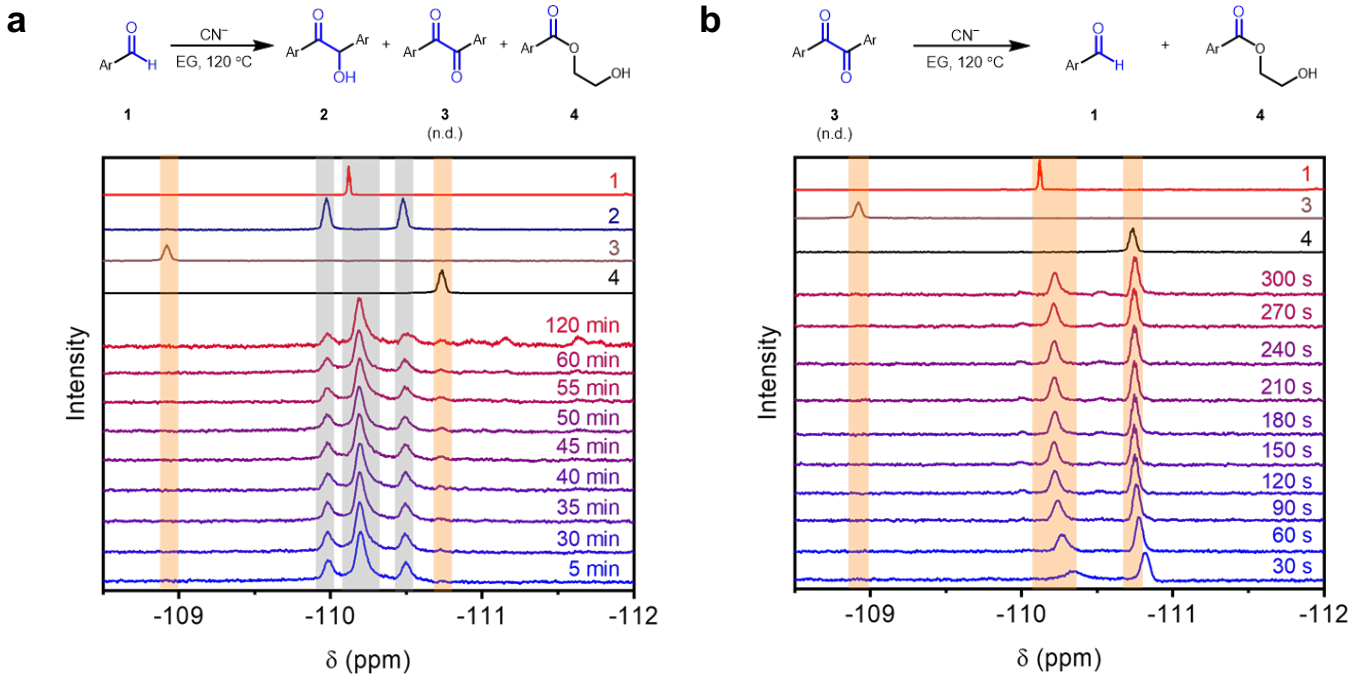

Figure 5. *In situ* ^{19}F NMR (470 MHz) studies of benzoin and benzil formation under the standard polymerization conditions. a) Time course of the reaction of **1**, showing that the benzoin condensation equilibrates very quickly (<5 min) to form **2** whereas the formation of **4** (presumably from **3**) is much slower. b) Kinetic investigation of the cyanolysis of **3** indicates that the conversion of **3** into **4** occurs nearly instantaneously under the reaction conditions. ^{19}F NMR was used in place of ^1H NMR for these studies due to the lack of diagnostic ^1H resonances for benzil species. An internal standard of 1-fluoronaphthalene was used for all ^{19}F NMR experiments (not shown). Ar = 3-fluorophenyl.

that predominantly benzil-linked polymers are fortuitously formed during the CN^--catalyzed polymerization of dialdehydes.

It should be noted that the IR spectrum of **poly(BPDA)** contains a diagnostic carbonyl C=O stretch (1675 cm^{-1}, broad), but the carbonyl stretches of benzoin (1679 cm^{-1}) and benzil (1657 cm^{-1}, with a shoulder at 1673 cm^{-1}) are nearly identical and thus cannot be used to distinguish between the two linkage chemistries (Figure 3b). Likewise, the stretch at 1374 cm^{-1} in **poly(BPDA)** could be attributed to an H–C–OH δ bend that is strong in benzoin, but this stretch is also present in benzil, and thus is not necessarily consistent with benzoin linkages either. As such, outside of the O–H stretch present in benzoin and absent in benzil and **poly(BPDA)**, IR spectroscopy is of limited use to distinguish between these two moieties. Similarly, Raman spectroscopy further supports that **poly(BPDA)** is a benzoin/benzil-linked polymer, but the spectra of the polymer and molecular analogues are sufficiently similar that they cannot be used to reliably distinguish between the two possible structures (SI Figure S40).

Mechanism of *in situ* benzoin oxidation. Given the reported oxidation of benzoin derivatives using O_2 and strong base,[48,49] we wondered if an initially formed benzoin-linked polymer was being oxidized by adventitious O_2 *in situ* or during the soaking process to yield benzil-linked **poly(BPDA)**. To test this possibility, **poly(BPDA)** was synthesized in a N_2-filled (<1 ppm O_2) glovebox **(poly(BPDA)-GB**) using freshly vacuum-distilled EG to rigorously ensure that the reaction, washes, soaks and drying steps were all conducted in an O_2-free environment (see SI section 4 for details). After drying, **poly(BPDA)-GB** was packed into an NMR rotor in the glovebox prior to analysis by CP MAS ^{13}C SSNMR under N_2. As shown in Figure 3a, **poly(BPDA)-GB** possesses a nearly identical ^{13}C NMR spectrum as that of **poly(BPDA)** synthesized outside of the glovebox. Likewise, the ATR-IR and UV-Vis spectra of **poly(BPDA)** and **poly(BPDA)-GB** are also very similar (Figures 3b–c). This finding confirms that adventitious O_2 is *not* required to form benzil-linked polymers, and that the *in situ* oxidation of benzoin linkages during the polymerization reaction must proceed via a mechanism that does not require O_2.

To gain further insight into the mechanism governing benzil formation under the standard polymerization conditions, molecular model studies were carried out using 3-fluorobenzaldehyde (**1**) as a surrogate for **BPDA** (Figure 4, SI Figure S90). Authentic samples of the possible products 3,3′-difluorobenzoin (**2**) and 3,3′-difluorobenzil (**3**) were prepared for comparison (see SI section 7a for details). Reactions were conducted for 30 min under air-free conditions using 1-fluoronapthalene as an internal standard (SI Figure S101; See SI section 7b for details). ^{19}F NMR was employed in place of ^1H NMR due to the lack of diagnostic ^1H NMR signals for benzil species. Subjecting **1** to the standard reaction conditions produced **2** along with other unidentified species (Figure 4a, SI Figure S91). However, **3** was not detected. Similarly, subjecting **2** to the same conditions produced a significant amount of **1** due to the reversibility of the benzoin reaction, but **3** was again not observed (Figure 4b, SI Figure S94). Notably, heating **2** in EG for 24 h in the absence

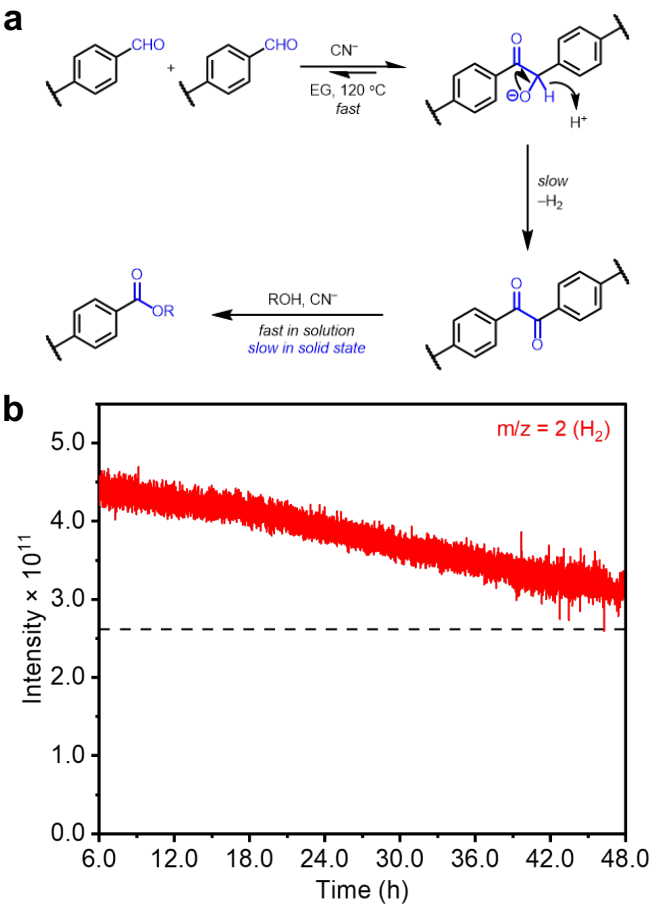

Figure 6. a) Proposed mechanism of benzil formation under the polymerization conditions. b) H_2 evolution detected by RGA during the polymerization of **BPDA** to **poly(BPDA)**. The dashed line corresponds to the background H_2 level detected from a "blank" reaction in which **BPDA** was excluded.

of CN^- produced only trace amounts of **3**, further supporting that adventitious O_2 alone is not responsible for benzil formation during the polymerization reaction (SI Figure S103). Synthesis of several potential side products (see SI Section 7a for details) confirmed that the major unidentified species in all cases was ester **4** formed from reaction with the solvent EG (Figure 4). Based on this finding, we inferred that **3** forms and rapidly undergoes cyanolysis via a previously reported pathway[50,51] to form **1** (which can react further to produce **2**) and **4** (see SI Figure S99 for a proposed mechanism). Indeed, subjecting **3** to the reaction conditions produced mostly **4**, along with small amounts of **1** and **2** (Figure 4c, SI Figure S97).

In situ ^{19}F NMR studies of the reaction of **1** with CN^- were next carried out to interrogate if **3** forms transiently under the reaction conditions prior to decomposition into **4** (Figure 5a). In these studies, the reaction mixture was transferred to a screw-cap NMR tube in a N_2-filled glovebox and then placed in an NMR spectrometer that had been preheated to 120 °C (see SI section 7c for details). Equilibration of **1** and **2** through the benzoin reaction occurred within the first 5 min of the reaction (Figure 5a, SI Figure S106). However, **3** was again not observed, even when the reaction was conducted for 24 h (SI Figures S107–S110). Notably, the

decomposition of the products was slower in an NMR tube, as even after 24 h, **1** and **2** were still detectable (SI Figure S109). This is likely due to a lack of mixing in the NMR tube.

To determine whether it is possible to observe **3** in the presence of CN^-, we subjected **3** to similar conditions as above in a screw-cap NMR tube (Figure 5b). Intriguingly, **3** was again not detected by ^{19}F NMR; instead, only **1** and **4** were observed in a 1:1.4 ratio. Consistently, although solid benzil could be observed in the NMR tube at room temperature, it was not sufficiently soluble in EG to be observed by ^{19}F-NMR, and any **3** that partially solubilized quickly converted to **4**, suggesting that the cyanolysis of **3** proceeds rapidly even at room temperature (SI Figure S113). Importantly, **4** was also observed in the reaction carried out with **1** (Figure 5a), although its generation was slower than the formation of **2** via the benzoin reaction.

We propose a kinetic scenario in which **1** and **2** rapidly equilibrate in the presence of CN^- via the benzoin reaction, followed by rate-limiting oxidation of **2** to **3** and subsequent rapid cyanolysis of **3** to **4** in solution (Figure 6a). In this kinetic regime, it would be nearly impossible to detect ~~**3 in solution**~~. Other than **1**, **2**, and **4**, the other species detected by ^{19}F NMR disappeared upon aqueous work-up (SI Figure S95), confirming that **1**, **2**, and **4** are the major isolable products formed under the reaction conditions. As further support that **BPDA** rapidly polymerizes via the benzoin reaction followed by slow oxidation to **poly(BPDA)**, ^1H NMR analysis of a polymerization in progress confirmed the formation of soluble benzoin species after only 30 min under the standard reaction conditions (SI Figure S187). Importantly, these findings suggest that the precipitation of insoluble **poly(BPDA)** during the polymerization is essential to the successful formation of benzil-linked polymers, as precipitation likely minimizes subsequent cyanolysis of the benzil linkages to form redox-inactive esters (SI Figure S131) [50,51]. This is supported by the absence of ester carbonyl resonances (δ ~160–180 ppm) in the SSNMR spectrum of **poly(BPDA)** (Figure 3a).

Based upon our finding that **4** (and, by implication, **3**) is only observed in the presence of CN^-, we hypothesized that CN^- is required for the *in situ* oxidation of benzoin linkages to benzils (Figure 6a). This process likely involves reversible deprotonation of the benzoin alcohol ($pK_a \approx 12$) by CN^- (pK_a of HCN ≈ 9) followed by hydride transfer, akin to the Cannizzaro reaction.[52] Consistently, previous computational studies have demonstrated that hydride transfer during the benzoin reaction is kinetically feasible,[53] and benzil formation in the nominal absence of O_2 has been observed experimentally as well.[49,54] The hydride acceptor could be a proton from the protic solvent to form H_2, another carbonyl group to form an alcohol (as in the Cannizzaro reaction), or adventitious O_2.[49] Comparison of the ^{19}F NMR spectra of model reactions (Figure 4) to those of 3-fluorobenzyl alcohol and 3,3′-difluorodihydrobenzoin suggests that these compounds are not present in any of the reaction mixtures, ruling out carbonyl-based hydride acceptors (Figure S92, see SI section 7 for details). Likewise, the formation of benzils under rigorously air-free conditions suggests that O_2 is also not required for benzoin oxidation. Critically, residual gas analysis (RGA) of the headspace of a polymerization reaction of **BPDA** in progress revealed significant H_2 formation above the background value (Figure 6b and SI Figures S115–S118; see SI section 8 for details). As such, the most likely scenario is that the solvent serves as a proton source to form H_2 upon hydride transfer (Figure 6a). This finding further supports that the hydride transfer is the rate-limiting step of benzil formation, as H_2 evolution was slow compared to the benzoin reaction (SI Figure 187). Nonetheless, more work is needed to elucidate the exact mechanism for *in situ* oxidation during the benzoin polymerization reaction.

Generality of benzil polymer synthesis. To expand the scope of this polymerization reaction and access materials with potentially improved electrical properties, we synthesized another 1,2-dione-linked polymer, termed **CORN-BP-2** and herein referred to as **poly(BTDA)**, from the bis(thiophene) linker **BTDA** under similar conditions (Figure 7a, see SI Section 5 for details). In both EtOH and EG, significant conversion of the monomer into **poly(BTDA)** was observed by ATR-IR (see SI Section 5 for details). Thus, the synthesis of **poly(BTDA)** was scaled up in both EG (**poly(BTDA)-EG**) and EtOH (**poly(BTDA)-EtOH**) for comparison, and these samples were characterized using the methods described above (see SI section 6 for details). Consistent with the findings for **poly(BPDA)**, CP MAS ^{13}C SSNMR and ATR-IR spectra support the formation of thenils instead of thenoins in both **poly(BTDA)** samples (Figure 8a–b). Specifically, CP MAS ^{13}C SSNMR revealed the absence of a H–^{13}C–OH resonance and much closer match of the carbonyl ^{13}C chemical shift (δ 178–180 ppm) in **poly(BTDA)** to that of thenil (δ 182.4 ppm) than to that of thenoin (δ 190.0 ppm) (SI Table S14). Furthermore, solid-state CV confirmed that **poly(BTDA)** undergoes two reversible one-electron reduction processes at 2.494V and 2.099 V vs. Li/Li^+, which are comparable to those of thenil at 2.434V and 2.008 V vs. Li/Li^+, respectively (Figure 8c, SI Figures S143 and S159, and Table S11).[23] Characterization of **poly(BTDA)** by SEM

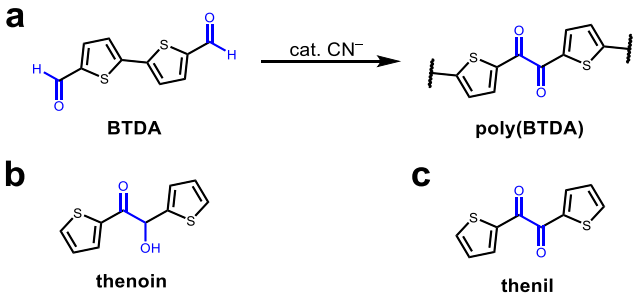

Figure 7. a) Conversion of **BTDA** to benzil-linked polymer **poly(BTDA)** under optimized reaction conditions. Model compounds b) 2,2′-thenoin and c) 2,2′-thenil.

(SI Figures S51–S52) and PXRD (SI Figure S66) demonstrated that it is also a microcrystalline polymeric material. Finally, characterization of **poly(BTDA)** by EDS and XPS revealed a lack of residual K from KCN (SI Figures S53–S54 and S59 and Table S7 and S9), but combustion analysis and XPS revealed trace N (~2%), possibly from residual nitrile groups incorporated during the polymerization (SI Tables S8–9). The successful synthesis of **poly(BTDA)** indicates

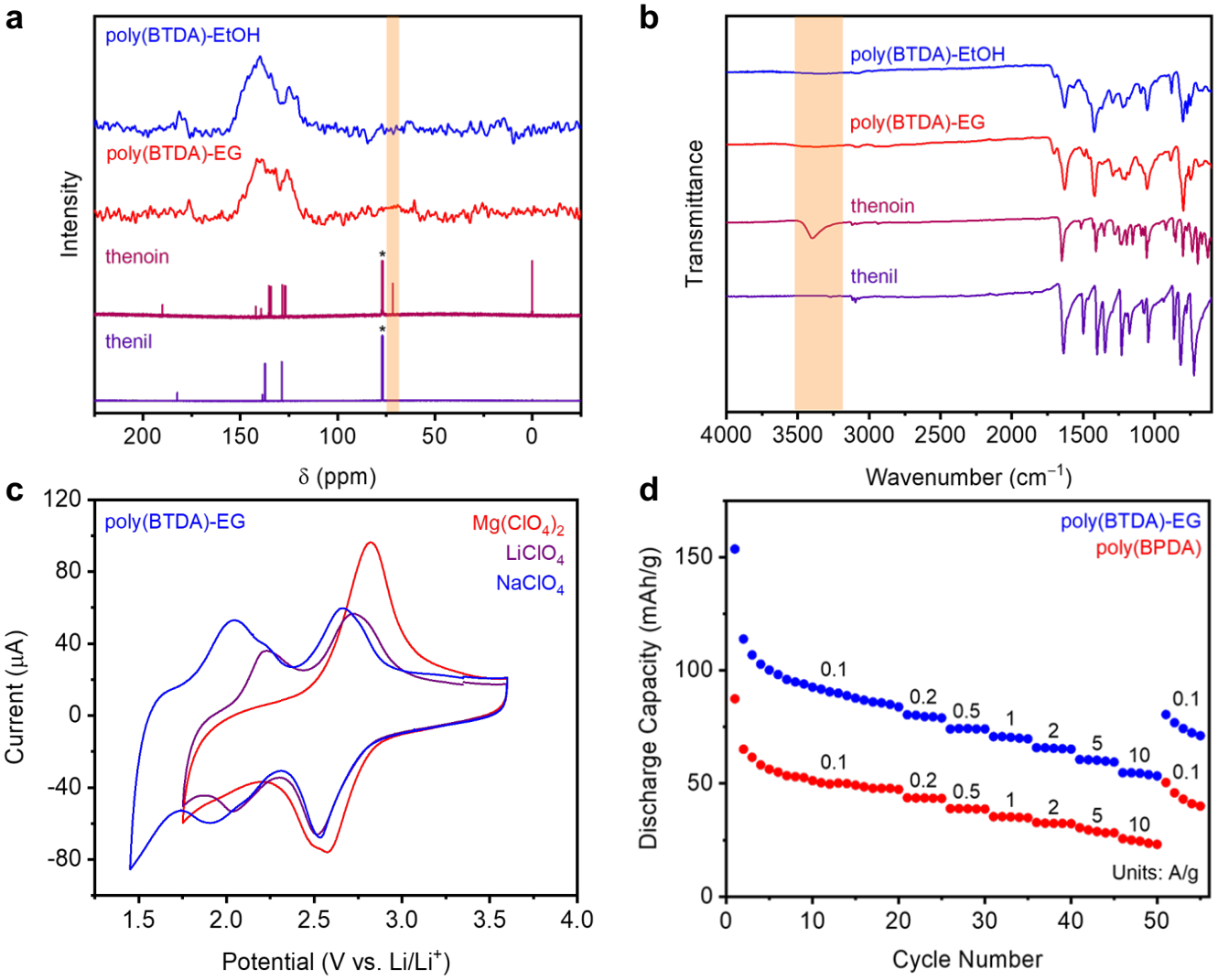

Figure 8. Solid-state spectroscopic and electrochemical characterizations of **poly(BTDA)-EG** prepared at 120 °C and **poly(BTDA)-EtOH** prepared at 80 °C with 0.50 equivalents of KCN for 96 h compared to model compounds 2,2′-thenoin and 2,2′-thenil. Electrochemical performance tests of **polymers** Battery composite: 60% **poly(BTDA)-EG** or **poly(BPDA)**, 30% CMK-3 carbon, 10% PVDF binder, unless specified otherwise. a) CP MAS ^{13}C-SSNMR (125 MHz) spectra of the polymers and solution-state ^{13}C NMR spectra (125 MHz, $CDCl_3$) of the model compounds. The peak corresponding to $CDCl_3$ is indicated (*). SSNMR spectra were collected at a spinning speed of 20 kHz with a ^{1}H–^{13}C contact time of 1 ms. The H–^{13}C–OH resonance of 2,2′-thenoin is highlighted. b) ATR IR spectra of polymers and model compounds. The O–H stretch of 2,2′-thenoin is highlighted. c) Solid-state CV of **poly(BTDA)-EG** carried out at 20 mV/s in 0.1 M $LiClO_4$, $NaClO_4$, and $(MgClO_4)_2$ in DMSO. d) Rate capability tests of battery composites carried out in 1.0 M LiTFSI in DMSO.

that the tandem benzoin-oxidation reaction is a general method for the synthesis of polymers linked predominantly by 1,2-diones.

Investigation of redox-activity. The high theoretical energy storage capacities of **poly(BPDA)** (257 mAh/g) and **poly(BTDA)** (243 mAh/g) make them attractive candidates for battery applications and competitive with other leading redox-active polymers such as P14AQ (theoretical capacity of 260 mAh/g, SI Table S12).[15] Thus, we investigated the potential of **poly(BPDA)** and **poly(BTDA)** as cathode materials in CR-2032 Li-metal half cells (see SI section 12 for details). This simple, well-behaved system allows us to probe useful properties such as long-term redox stability and fast charge/discharge capabilities in a standardized manner. Each polymer's performance was first assessed using composite electrodes containing 30% active material, 60% CMK-3, and 10% polyvinylidene difluoride (PVDF) binder using 1.0 M LiTFSI in DMSO as the electrolyte solution (see SI section 12 for details). Although **poly(BPDA)** demonstrated promising capacities (up to 134 mAh/g) in preliminary tests, continued cycling resulted in significant capacity losses (SI Figure S155). Gratifyingly, **poly(BTDA)-EG** demonstrated similar initial capacity (124 mAh/g, Figure 8b) and rate capabilities as **poly(BPDA)** (Figure S154), but with improved capacity retention upon cycling (67% vs. 45% after 100 cycles). Notably, ^{1}H-NMR analysis confirmed the extremely poor solubility of neutral **poly(BTDA)** in DMSO-d_6 (SI Figure S170), potentially explaining its improved cycling stability.

Both samples were further tested as composites with 60% active material, 30% CMK-3, and 10% PVDF binder, a composition that is more reflective of actual organic electrode materials (Table S12). The behavior of **poly(BTDA)-EG** at high active mass loading was evaluated by assessing its capacity retention at faster discharge rates (Figure 8d) and its cycling stability (SI Figure S163). Promisingly, **poly(BTDA)-EG** retained 64% of its capacity when the discharge rate was increased 100-fold from 0.10 A/g (84 mAh/g) to 10 A/g (54 mAh/g), using the twentieth cycle capacity at 0.10 A/g for comparison (Figure 8d). After five discharge cycles at 10 A/g, >87% (74 mAh/g) of the original capacity was recovered when the discharge rate was returned to 0.10 A/g. Similarly, in cycling studies at a discharge rate of 50 mA/g, **poly(BTDA)-EG** retained 73% of its capacity between the 10th and 100th cycles (Figure S162). The performance of **poly(BTDA)-EG** at different rates was also superior to that of **poly(BPDA)** (Figure 8d), reflecting the advantage of being able to readily tune the flanking aryl groups of the 1,2-dione units using our polymerization strategy.

We hypothesize that the observed capacity losses for **poly(BTDA)-EG** in both cycling and rate tests is due to partial dissolution of the material during charging and discharging, which is a well-known challenge for organic electrode materials.[55–60] This is further suggested by the post-mortem CVs of both **poly(BPDA)** and **poly(BTDA)-EG** (SI Figures S173–S174), which indicate that the redox-activity of both polymers is maintained after 100 cycles. In addition, slight discoloration was observed in the electrolyte solution of disassembled cells after cycling. Other possible causes for the observed deviation from the theoretical capacities of these materials include undetected trace benzoin linkages contributing to irreversible capacity, inactive terminal esters contributing dead weight, and/or the inability of the polymer to efficiently stabilize the negative charge associated with the fully reduced species. In future work, we will alleviate the partial solubility of these materials by cross-linking or by incorporation into polymeric networks,[55,56,61–64] which are common methods to overcome this problem in redox-active organic materials.

One of the most exciting features of organic electrode materials is that they can be readily adapted to work with almost any cation, including those such as Na^+ and Mg^{2+} that are more abundant than Li^+,[65–67] and their redox properties can be optimized by tuning hard-soft acid-base interactions.[68–70] Indeed, previous molecular studies have demonstrated that 1,2-diones are promising potential electrode materials for Mg-ion batteries, because the two one-electron waves observed with monovalent cations such as Li^+ collapse into a single two-electron reduction wave with Mg^{2+} cations due to the excellent hard-hard match of the divalent cation and the reduced carbonyl groups.[29] However, this promising feature has not been demonstrated in polymeric electrode materials to date.

To probe the potential suitability of **poly(BTDA)-EG** for electrochemical energy storage or electrocatalysis with alternative ions, CVs were carried out with various electrolytes (0.1 M $LiClO_4$, $NaClO_4$, $KClO_4$, $^nBu_4NClO_4$, and $Mg(ClO_4)_2$ in DMSO) at a sweep rate of 20 mV/s using a standard 3-electrode set-up in a N_2-filled glovebox (Figure 8c, SI Figures S175–S182). The data for Li^+, Na^+, and Mg^{2+} are included in Figure 8c for clarity. Importantly, the reduction potentials measured for Li^+ by CV were nearly identical between the 3-electrode set-up and in the CR-2032 half cells (Figure 8c, SI Figures S159 and S175, Tables S11 and S13).

Changing cations had little impact on the potential of the first reduction peak, with the biggest difference (120 mV, 11.6 kJ/mol) observed between hard Mg^{2+} and soft K^+ (SI Figure S180 and Table S13). The change in behavior was much more drastic for the second reduction peak potentials among the monovalent cations. Decreasing the charge density (*i.e.*, increasing the size) of the monovalent cation from Li^+ to $^nBu_4N^+$ resulted in a decrease in the magnitude of the second reduction potential, from 2.031 V (Li^+) to 1.899 V (Na^+) to 1.740 V (K^+) and 1.773 V ($^nBu_4N^+$) vs. Li/Li^+, respectively (SI Table S13, see section 12 for further discussion on $^nBu_4N^+$). This finding suggests that among monovalent cations, Li^+ best stabilizes the doubly reduced form of **poly(BTDA)-EG** due to the hard-hard match of the reduced carbonyl units and the Li^+ cations.[29,68–70]

Intriguingly, switching from monovalent cations to divalent Mg^{2+} caused the second reduction peak to dramatically shift to 2.501 V vs. Li/Li^+, leading the second reduction peak to almost merge with the first peak to reveal a nearly simultaneous two-electron transfer (Figure 8c). This finding suggests that Mg^{2+} best stabilizes doubly reduced **poly(BTDA)-EG**. Furthermore, the redox-activity of **poly(BTDA)-EG** was better retained over 100 CV cycles with Mg^{2+} compared to Li^+, indicating Mg^{2+} also best minimizes solubilization of the reduced polymer (SI Figures S181–S182, see SI section 12 for further discussion). This finding suggests that 1,2-dione-linked polymers may be promising organic electrode materials for incorporation into next-generation Mg-ion batteries, which we will explore in future work.

The tunability of the reduction potentials of dione-based polymers through exploiting hard-soft acid-base matching between the charge-compensating cation and reduced polymer is consistent with previous studies in other systems.[29,69,71,72] This tunability allows for a single versatile structure to be employed for applications requiring alternative ions without having to design a specific material for each cation.

CONCLUSION

The development of sustainable methods for the scalable synthesis of redox-active organic materials represents a fundamental barrier to the deployment of next-generation organic electrode materials. During the attempted synthesis of benzoin-linked polymers, herein we report the serendipitous discovery that the cyanide-catalyzed polymerization of dialdehydes leads to redox-active 1,2-dione-linked materials instead. These results demonstrate that the benzoin reaction is a viable method for the sustainable synthesis of modular, redox-active polymers. Furthermore, our electrochemical studies reveal that 1,2-dione-linked materials such as **poly(BTDA)** are viable candidates for electrochemical energy storage due to their promising cycling stability and good retention of capacity at fast discharge rates. Intriguingly, the use of CN^- in molecular systems also results in

low yields of the desired benzoin products, because of potential *in situ* oxidation and cyanolysis, even under rigorously air-free conditions, a phenomenon previously unreported or attributed to adventitious oxygen.[48,54] Therefore, our findings also have important potential implications for related reactions involving cyanide and other nucleophilic catalysts in combination with aldehydic substrates.[35,36] Future work will focus on moving away from CN^- catalysts due to their toxicity, minimizing the solubility of these materials through cross-linking or incorporation of 1,2-diones into less soluble materials such as polymer networks or covalent organic frameworks, decreasing the conductive additives in battery composites by improving the intrinsic conductivity of these materials, and further optimizing their redox activities. Furthermore, the potential of these redox-active materials for electrocatalysis will be evaluated.

ASSOCIATED CONTENT

Supporting Information. Full characterization and electrochemical data. This material is available free of charge via the Internet at http://pubs.acs.org.

AUTHOR INFORMATION

Corresponding Author

*pjm347@cornell.edu

Author Contributions

P.J.M. devised the project. J.K. and C.C. synthesized and characterized all molecular and polymeric samples. C.N.G. and H.D.A. carried out all electrochemical measurements and analyses, with the exception of some CV measurements that were carried out by J.K. The manuscript was written through contributions of all authors, and all authors have given approval to the final version of the manuscript.

‡These authors contributed equally.

Funding Sources

We thank Cornell University for initial financial support of this work and for providing a Summer Experience Grant to C. C. The development of redox-active materials with potential applications in heterogeneous electrocatalysis was supported by the National Institute of General Medical Sciences of the National Institutes of Health under award number R35GM138165 (C. C., J. K., P. J. M.). The content is solely the responsibility of the authors and does not necessarily represent the official views of the National Institutes of Health. C. N. G. and H. D. A. thank the National Science Foundation Center for Synthetic Organic Electrochemistry (CHE-2002158) and Mercedes Benz for funding. This work made use of the Cornell Center for Materials Research Shared Facilities, which are supported through the NSF MRSEC program (DMR-1719875). ^{1}H NMR data were collected on a Bruker INOVA 500 MHz spectrometer that was purchased with support from the NSF (CHE-1531632).

ACKNOWLEDGMENT

We thank Drs. Ivan Keresztes (Cornell University) and Alexander C. Forse (University of Cambridge) for assistance with solid-state NMR experiments and Prof. Brett Fors (Cornell University) and Dr. Brian Peterson (Cornell University) for helpful discussions. We thank Nathan Lui (Cornell University) and Prof. David Collum (Cornell University) for assistance with preliminary density functional theory calculations.

REFERENCES

(1) *Climate Change 2014: Synthesis Report*; Pachauri, R. K., Mayer, L., Intergovernmental Panel on Climate Change, Eds.; Intergovernmental Panel on Climate Change: Geneva, Switzerland, 2015.

(2) *CO_2 Emissions from Fuel Combustion: Overview*; International Energy Agency: Paris, France, 2017.

(3) Denholm, P.; Ela, E.; Kirby, B.; Milligan, M. The Role of Energy Storage with Renewable Electricity Generation. *Energy Storage: Issues and Applications* **2011**, No. January, 1–58.

(4) Novaes, L. F. T.; Liu, J.; Shen, Y.; Lu, L.; Meinhardt, J. M.; Lin, S. Electrocatalysis as an Enabling Technology for Organic Synthesis. *Chem. Soc. Rev.* **2021**, *50* (14), 7941–8002. https://doi.org/10.1039/D1CS00223F.

(5) Rajeev, R.; Sharma, B.; Mathew, A. T.; George, L.; Y N, S.; Varghese, A. Review—Electrocatalytic Oxidation of Alcohols Using Chemically Modified Electrodes: A Review. *J. Electrochem. Soc.* **2020**, *167* (13), 136508. https://doi.org/10.1149/1945-7111/abb9d0.

(6) Voskian, S.; Hatton, T. A. Faradaic Electro-Swing Reactive Adsorption for CO_2 Capture. *Energy Environ. Sci.* **2019**, *12* (12), 3530–3547. https://doi.org/10.1039/C9EE02412C.

(7) Dey, A.; Gunnoe, T. B.; Stamenkovic, V. R. Organic Electrosynthesis: When Is It Electrocatalysis? *ACS Catal.* **2020**, *10* (21), 13156–13158. https://doi.org/10.1021/acscatal.0c04559.

(8) Malinauskas, A. Electrocatalysis at Conducting Polymers. *Synthetic Metals* **1999**, *107* (2), 75–83. https://doi.org/10.1016/S0379-6779(99)00170-8.

(9) Zhao, X.; Pachfule, P.; Thomas, A. Covalent Organic Frameworks (COFs) for Electrochemical Applications. *Chem. Soc. Rev.* **2021**, *50* (12), 6871–6913. https://doi.org/10.1039/D0CS01569E.

(10) Nitopi, S.; Bertheussen, E.; Scott, S. B.; Liu, X.; Engstfeld, A. K.; Horch, S.; Seger, B.; Stephens, I. E. L.; Chan, K.; Hahn, C.; Nørskov, J. K.; Jaramillo, T. F.; Chorkendorff, I. Progress and Perspectives of Electrochemical CO_2 Reduction on Copper in Aqueous Electrolyte. *Chem. Rev.* **2019**, *119* (12), 7610–7672. https://doi.org/10.1021/acs.chemrev.8b00705.

(11) Yazdani, A.; Botte, G. G. Perspectives of Electrocatalysis in the Chemical Industry: A Platform for Energy Storage. *Current Opinion in Chemical Engineering* **2020**, *29*, 89–95. https://doi.org/10.1016/j.coche.2020.07.003.

(12) Masias, A.; Marcicki, J.; Paxton, W. A. Opportunities and Challenges of Lithium Ion Batteries in Automotive Applications. *ACS Energy Lett.* **2021**, *6* (2), 621–630. https://doi.org/10.1021/acsenergylett.0c02584.

(13) Larcher, D.; Tarascon, J. M. Towards Greener and More Sustainable Batteries for Electrical Energy Storage. *Nat. Chem.* **2015**, *7* (1), 19–29. https://doi.org/10.1038/nchem.2085.

(14) Poizot, P.; Dolhem, F. Clean Energy New Deal for a Sustainable World: From Non-CO_2 Generating Energy Sources to Greener Electrochemical Storage Devices. *Energy Environ. Sci.* **2011**, *4* (6), 2003–2019. https://doi.org/10.1039/c0ee00731e.

(15) Esser, B.; Dolhem, F.; Becuwe, M.; Poizot, P.; Vlad, A.; Brandell, D. A Perspective on Organic Electrode

Materials and Technologies for next Generation Batteries. *J. Power Sources* **2021**, *482* (October 2020), 228814. https://doi.org/10.1016/j.jpowsour.2020.228814.

(16) Gannett, C. N.; Melecio-Zambrano, L.; Theibault, M. J.; Peterson, B. M.; Fors, B. P.; Abruña, H. D. Organic Electrode Materials for Fast-Rate, High-Power Battery Applications. *Materials Reports: Energy* **2021**, *1* (1), 100008. https://doi.org/10.1016/j.matre.2021.01.003.

(17) Lu, Y.; Zhang, Q.; Li, L.; Niu, Z.; Chen, J. Design Strategies toward Enhancing the Performance of Organic Electrode Materials in Metal-Ion Batteries. *Chem* **2018**, *4* (12), 2786–2813. https://doi.org/10.1016/j.chempr.2018.09.005.

(18) Muench, S.; Wild, A.; Friebe, C.; Häupler, B.; Janoschka, T.; Schubert, U. S. Polymer-Based Organic Batteries. *Chem. Rev.* **2016**, *116* (16), 9438–9484. https://doi.org/10.1021/acs.chemrev.6b00070.

(19) Lee, S.; Kwon, G.; Ku, K.; Yoon, K.; Jung, S. K.; Lim, H. D.; Kang, K. Recent Progress in Organic Electrodes for Li and Na Rechargeable Batteries. *Adv. Mater.* **2018**, *30* (42), 1–45. https://doi.org/10.1002/adma.201704682.

(20) Schon, T. B.; McAllister, B. T.; Li, P. F.; Seferos, D. S. The Rise of Organic Electrode Materials for Energy Storage. *Chem. Soc. Rev.* **2016**, *45* (22), 6345–6404. https://doi.org/10.1039/c6cs00173d.

(21) An, S. Y.; Tyler, |; Schon, B.; Bryony, |; Mcallister, T.; Seferos, D. S. Design Strategies for Organic Carbonyl Materials for Energy Storage: Small Molecules, Oligomers, Polymers and Supramolecular Structures. *EcoMat* **2020**, *2* (4), e12055. https://doi.org/10.1002/eom2.12055.

(22) Sieuw, L.; Jouhara, A.; Quarez, E.; Auger, C.; Gohy, J.-F.; Poizot, P.; Vlad, A. A H-Bond Stabilized Quinone Electrode Material for Li-Organic Batteries: The Strength of Weak Bonds. *Chem. Sci.* **2019**, *10*, 418–426. https://doi.org/10.1039/c8sc02995d.

(23) Ma, T.; ing Zhao, Q.; Wang, J.; Pan, Z. A Sulfur Heterocyclic Quinone Cathode and A Multifunctional Binder for A High-Performance Rechargeable Lithium-Ion Battery. *Angew. Chem. Int. Ed.* **2016**, *55* (22), 6428–6432. https://doi.org/10.1002/ange.201601119.

(24) Miroshnikov, M.; Mahankali, K.; Thangavel, K. N.; Satapathy, S.; Reddya, L. M.; Ajayan, P. M.; Ohn, G. Bioderived Molecular Electrodes for Next-Generation Energy-Storage Materials. *ChemSusChem* **2020**, 2186–2204. https://doi.org/10.1002/cssc.201903589.

(25) Chen, H.; Armand, M.; Demailly, G.; Dolhem, F.; Poizot, P.; Tarascon, J.-M. From Biomass to a Renewable $Li_XC_6O_6$ Organic Electrode for Sustainable Li-Ion Batteries. *ChemSusChem* **2008**, *1* (4), 348–355. https://doi.org/10.1002/cssc.200700161.

(26) Amin, K.; Mao, L.; Wei, Z. Recent Progress in Polymeric Carbonyl-Based Electrode Materials for Lithium and Sodium Ion Batteries. *Macromol. Rapid Commun.* **2019**, *40* (1), 1–25. https://doi.org/10.1002/marc.201800565.

(27) Hahn, S.; Alrayyani, M.; Sontheim, A.; Wang, X.; Rominger, F.; Miljanić, O.; Bunz, U. H. F. Synthesis and Characterization of Heterobenzenacyclo-Octaphanes Derived from Cyclotetrabenzoin. *Chem. Eur. J.* **2017**, *23* (44), 10543–10550. https://doi.org/10.1002/chem.201701125.

(28) Shimizu, A.; Kuramoto, H.; Tsujii, Y.; Nokami, T.; Inatomi, Y.; Hojo, N.; Suzuki, H.; Yoshida, J. I. Introduction of Two Lithiooxycarbonyl Groups Enhances Cyclability of Lithium Batteries with Organic Cathode Materials. *J. Power Sources* **2014**, *260*, 211–217. https://doi.org/10.1016/j.jpowsour.2014.03.027.

(29) Hernández-Burgos, K.; Rodríguez-Calero, G. G.; Zhou, W.; Burkhardt, S. E.; Abruña, H. D. Increasing the Gravimetric Energy Density of Organic Based Secondary Battery Cathodes Using Small Radius Cations (Li^+ and Mg^{2+}). *J. Am. Chem. Soc.* **2013**, *135* (39), 14532–14535. https://doi.org/10.1021/ja407273c.

(30) Liang, Y.; Zhang, P.; Chen, J. Function-Oriented Design of Conjugated Carbonyl Compound Electrodes for High Energy Lithium Batteries. *Chem. Sci.* **2013**, *4* (3), 1330–1337. https://doi.org/10.1039/c3sc22093a.

(31) Nokami, T.; Matsuo, T.; Inatomi, Y.; Hojo, N.; Tsukagoshi, T.; Yoshizawa, H.; Shimizu, A.; Kuramoto, H.; Komae, K.; Tsuyama, H.; Yoshida, J. I. Polymer-Bound Pyrene-4,5,9,10-Tetraone for Fast-Charge and -Discharge Lithium-Ion Batteries with High Capacity. *J. Am. Chem. Soc.* **2012**, *134* (48), 19694–19700. https://doi.org/10.1021/ja306663g.

(32) Gao, H.; Neale, A. R.; Zhu, Q.; Bahri, M.; Wang, X.; Yang, H.; Xu, Y.; Clowes, R.; Browning, N. D.; Little, M. A.; Hardwick, L. J.; Cooper, A. I. A Pyrene-4,5,9,10-Tetraone-Based Covalent Organic Framework Delivers High Specific Capacity as a Li-Ion Positive Electrode. *J. Am. Chem. Soc.* **2022**, *144* (21), 9434–9442. https://doi.org/10.1021/jacs.2c02196.

(33) Zheng, S.; Miao, L.; Sun, T.; Li, L.; Ma, T.; Bao, J.; Tao, Z.; Chen, J. An Extended Carbonyl-Rich Conjugated Polymer Cathode for High-Capacity Lithium-Ion Batteries. *J. Mater. Chem. A* **2021**, *9* (5), 2700–2705. https://doi.org/10.1039/D0TA11648C.

(34) Tang, M.; Li, H.; Wang, E.; Wang, C. Carbonyl Polymeric Electrode Materials for Metal-Ion Batteries. *Chin. Chem. Lett.* **2018**, *29* (2), 232–244. https://doi.org/10.1016/j.cclet.2017.09.005.

(35) Kieslich, D.; Christoffers, J. Cyanide Anions as Nucleophilic Catalysts in Organic Synthesis. *Synthesis (Germany)* **2021**, *53* (19), 3485–3496. https://doi.org/10.1055/a-1499-8943.

(36) Menon, R. S.; Biju, A. T.; Nair, V. Recent Advances in N-Heterocyclic Carbene (NHC)-Catalysed Benzoin Reactions. *Beilstein J. Org. Chem.* **2016**, *12*, 444–461. https://doi.org/10.3762/bjoc.12.47.

(37) Wöhler; Liebig. Untersuchungen über das Radikal der Benzoesäure. *Ann. Pharm.* **1832**, *3* (3), 249–282. https://doi.org/10.1002/jlac.18320030302.

(38) ADB-ALLA, M. Novel Synthesis of Poly(Benzoin) and Poly(Benzil). Characterization and Application as Phtosensitizer Materials. *Macromol. Chem. Phys.* **1991**, *192* (2), 277–283. https://doi.org/10.1002/macp.1991.021920209.

(39) Weiss, M.; Appel, M. The Catalytic Oxidation of Benzoin to Benzil. *J. Am. Chem. Soc.* **1948**, *70* (11), 3666–3667. https://doi.org/10.1021/ja01191a036.

(40) Ashirov, T.; Alrayyani, M.; Song, K.-S.; Miljanić, O. Š.; Coskun, A. Cyclotetrabenzil-Based Porous Organic Polymers with High Carbon Dioxide Affinity. *Organic*

Materials **2021**, *03* (02), 346–352. https://doi.org/10.1055/a-1512-5753.

(41) Alrayyani, M.; Miljanić, O. Benzoins and Cyclobenzoins in Supramolecular and Polymer Chemistry. *Chem. Commun.* **2018**, *54* (85), 11989–11997. https://doi.org/10.1039/c8cc07407k.

(42) Pinaud, J.; Vijayakrishna, K.; Taton, D.; Gnanou, Y. Step-Growth Polymerization of Terephthaldehyde Catalyzed by N-Heterocyclic Carbenes. *Macromolecules* **2009**, *42* (14), 4932–4936. https://doi.org/10.1021/ma900907f.

(43) Byrne, F. P.; Jin, S.; Paggiola, G.; Petchey, T. H. M.; Clark, J. H.; Farmer, T. J.; Hunt, A. J.; Robert McElroy, C.; Sherwood, J. Tools and Techniques for Solvent Selection: Green Solvent Selection Guides. *Sustain. Chem. Process.* **2016**, *4* (1), 1–24. https://doi.org/10.1186/s40508-016-0051-z.

(44) Yamamoto, T.; Komarudin, D.; Arai, M.; Lee, B.-L.; Suganuma, H.; Asakawa, N.; Inoue, Y.; Kubota, K.; Sasaki, S.; Fukuda, T.; Matsuda, H. Extensive Studies on π-Stacking of Poly(3-Alkylthiophene-2,5-Diyl)s and Poly(4-Alkylthiazole-2,5-Diyl)s by Optical Spectroscopy, NMR Analysis, Light Scattering Analysis, and X-Ray Crystallography. *J. Am. Chem. Soc.* **1998**, *120* (9), 2047–2058.

(45) Rovnyak, D. Tutorial on Analytic Theory for Cross-Polarization in Solid State NMR. *Concepts Magn. Reson.* **2008**, *32A* (4), 254–276. https://doi.org/10.1002/cmr.a.20115.

(46) Park, S. Y.; Kang, C. W.; Lee, S. M.; Kim, H. J.; Ko, Y. J.; Choi, J.; Son, S. U. Nanoparticulate Conjugated Microporous Polymer with Post-Modified Benzils for Enhanced Pseudocapacitor Performance. *Chem. Eur. J.* **2020**, *26* (54), 12343–12348. https://doi.org/10.1002/chem.202002311.

(47) Chandrasekaran, M.; Noel, M.; Krishnan, V. Voltammetric Behaviour of Benzil at a Glassy Carbon Electrode. *J. Chem. Soc., Perkin Trans. 1* **1992**, 6, 979–985. https://doi.org/10.1039/p29920000979.

(48) Satyam, K.; Ramarao, J.; Suresh, S. N-Heterocyclic Carbene (NHC)-Catalyzed Intramolecular Benzoin Condensation-Oxidation. *Org. Biomol. Chem.* **2021**, *19* (7), 1488–1492. https://doi.org/10.1039/d0ob02606a.

(49) Shimakawa, Y.; Morikawa, T.; Sakaguchi, S. Facile Route to Benzils from Aldehydes via NHC-Catalyzed Benzoin Condensation under Metal-Free Conditions. *Tetrahedron Lett.* **2010**, *51* (13), 1786–1789. https://doi.org/10.1016/j.tetlet.2010.01.103.

(50) Cho, D. G.; Jong, H. K.; Sessler, J. L. The Benzil-Cyanide Reaction and Its Application to the Development of a Selective Cyanide Anion Indicator. *J. Am. Chem. Soc.* **2008**, *130* (36), 12163–12167. https://doi.org/10.1021/ja8039025.

(51) Kwart, H.; Baevsky, M. M. The Cyanide Ion Catalyzed Cleavage of Aromatic α-Diketones. *J. Am. Chem. Soc.* **1958**, *80* (3), 580–588. https://doi.org/10.1021/ja01536a018.

(52) Cannizzaro, S. Ueber Den Der Benzoësäure Entsprechenden Alkohol. *Justus Liebigs Annalen der Chemie* **1853**, *88* (1), 129–130. https://doi.org/10.1002/jlac.18530880114.

(53) Yamabe, S.; Yamazaki, S. Three Competitive Transition States in the Benzoin Condensation Compared to the Clear Rate-Determining Step in the Cannizzaro Reaction. *Org. Biomol. Chem.* **2009**, *7* (5), 951. https://doi.org/10.1039/b817849f.

(54) Yang, Z.; Wong, H. N. C.; Hon, P. M.; Chang, H. M.; Lee, C. M. A Novel Synthesis of the Dibenz[6,/]Oxepin Ring System: 10,11-Dihydro-11-Hydroxydibenz[6,/]Oxepin-10(l 117)-One. *J. Org. Chem* **1992**, *57* (14), 4033–4034. https://doi.org/10.1021/jo00040a059.

(55) Peterson, B. M.; Ren, D.; Shen, L.; Wu, Y. C. M.; Ulgut, B.; Coates, G. W.; Abruna, H. D.; Fors, B. P. Phenothiazine-Based Polymer Cathode Materials with Ultrahigh Power Densities for Lithium Ion Batteries. *ACS Applied Energy Materials* **2018**, *1* (8), 3560–3564. https://doi.org/10.1021/acsaem.8b00778.

(56) Gannett, C. N.; Peterson, B. M.; Shen, L.; Seok, J.; Fors, B. P.; Abruña, H. D. Cross-linking Effects on Performance Metrics of Phenazine-Based Polymer Cathodes. *ChemSusChem* **2020**, *13* (9), 2428–2435. https://doi.org/10.1002/cssc.201903243.

(57) Peng, C.; Ning, G.-H.; Su, J.; Zhong, G.; Tang, W.; Tian, B.; Su, C.; Yu, D.; Zu, L.; Yang, J.; Ng, M.-F.; Hu, Y.-S.; Yang, Y.; Armand, M.; Loh, K. P. Reversible Multi-Electron Redox Chemistry of π-Conjugated N-Containing Heteroaromatic Molecule-Based Organic Cathodes. *Nat. Energy* **2017**, *2* (7), 17074. https://doi.org/10.1038/nenergy.2017.74.

(58) Verdejo, R.; Bernal, M. M.; Romasanta, L. J.; Lopez-Manchado, M. A. Graphene Filled Polymer Nanocomposites. *J. Mater. Chem.* **2011**, *21* (10), 3301–3310. https://doi.org/10.1039/C0JM02708A.

(59) Nisula, M.; Karppinen, M. *In Situ* Lithiated Quinone Cathode for ALD/MLD-Fabricated High-Power Thin-Film Battery. *J. Mater. Chem. A* **2018**, *6* (16), 7027–7033. https://doi.org/10.1039/C8TA00804C.

(60) Suga, T.; Konishi, H.; Nishide, H. Photocrosslinked Nitroxide Polymer Cathode-Active Materials for Application in an Organic-Based Paper Battery. *Chem. Commun.* **2007**, No. 17, 1730. https://doi.org/10.1039/b618710b.

(61) Tan, S.-J.; Zeng, X.-X.; Ma, Q.; Wu, X.-W.; Guo, Y.-G. Recent Advancements in Polymer-Based Composite Electrolytes for Rechargeable Lithium Batteries. *Electrochem. Energ. Rev.* **2018**, *1* (2), 113–138. https://doi.org/10.1007/s41918-018-0011-2.

(62) Dirlam, P. T.; Glass, R. S.; Char, K.; Pyun, J. The Use of Polymers in Li-S Batteries: A Review. *J. Polym. Sci. Part A: Polym. Chem.* **2017**, *55* (10), 1635–1668. https://doi.org/10.1002/pola.28551.

(63) Lopez, J.; Mackanic, D. G.; Cui, Y.; Bao, Z. Designing Polymers for Advanced Battery Chemistries. *Nat. Rev. Mater.* **2019**, *4* (5), 312–330. https://doi.org/10.1038/s41578-019-0103-6.

(64) Gannett, C. N.; Peterson, B. M.; Melecio-Zambrano, L.; Trainor, C. Q.; Fors, B. P.; Abruña, H. D. Performance Optimization and Fast Rate Capabilities of Novel Polymer Cathode Materials through Balanced Electronic and Ionic Transport. *J. Mater. Chem. A* **2021**, *9* (9), 5657–5663. https://doi.org/10.1039/D0TA11099J.

(65) Haynes, W. M. Abundance of Elements in the Earth's Crust and in the Sea. In *CRC Handbook of Chemistry and Physics*; Lide, D. R., Bruno, Thomas J., Eds.; CRC Press; pp 14–17.

(66) Walter, M.; Kravchyk, K. V.; Ibáñez, M.; Kovalenko, M. V. Efficient and Inexpensive Sodium–Magnesium Hybrid

Battery. *Chem. Mater.* **2015**, *27* (21), 7452–7458. https://doi.org/10.1021/acs.chemmater.5b03531.

(67) Ma, D.; Zhao, H.; Cao, F.; Zhao, H.; Li, J.; Wang, L.; Liu, K. A Carbonyl-Rich Covalent Organic Framework as a High-Performance Cathode Material for Aqueous Rechargeable Zinc-Ion Batteries. *Chem. Sci.* **2022**, *13* (8), 2385–2390. https://doi.org/10.1039/D1SC06412F.

(68) Pearson, R. G. Hard and Soft Acids and Bases. *J. Am. Chem. Soc.* **1963**, *85* (22), 3533–3539.

(69) Ji, X. A Paradigm of Storage Batteries. *Energy Environ. Sci.* **2019**, *12* (11), 3203–3224. https://doi.org/10.1039/C9EE02356A.

(70) Gannett, C. N.; Kim, J.; Tirtariyadi, D.; Abruña, H. D.; Milner, P. J. Investigation of Ion-Electrode Interactions of Linear Polyimides and Alkali Metal Ions for Next Generation Alternative-Ion Batteries. *Chem. Sci.* **2022**. https://doi.org/10.1039/C7SC03842A.

(71) Wu, X.; Markir, A.; Ma, L.; Xu, Y.; Jiang, H.; Leonard, D. P.; Shin, W.; Wu, T.; Lu, J.; Ji, X. A Four-Electron Sulfur Electrode Hosting a Cu^{2+}/Cu^{+} Redox Charge Carrier. *Angew. Chem. Int. Ed.* **2019**, *58* (36), 12640–12645. https://doi.org/10.1002/anie.201905875.

(72) Dong, S.; Shin, W.; Jiang, H.; Wu, X.; Li, Z.; Holoubek, J.; Stickle, W. F.; Key, B.; Liu, C.; Lu, J.; Greaney, P. Alex.; Zhang, X.; Ji, X. Ultra-Fast NH_4^+ Storage: Strong H Bonding between NH_4^+ and Bi-Layered V_2O_5. *Chem* **2019**, *5* (6), 1537–1551. https://doi.org/10.1016/j.chempr.2019.03.009.

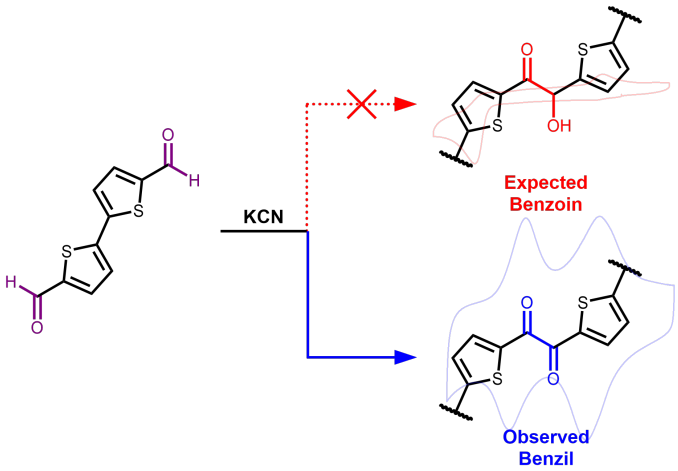
KCN
Expected
Benzoin
Observed
Benzil